Three-dimensional waveform modeling of ionospheric signature induced by the 2004 Sumatra tsunami

Giovanni Occhipinti, Philippe Lognonné, E. Alam Kherani, Hélène Hébert

Three-dimensional waveform modeling of ionospheric signature induced by the 2004 Sumatra tsunami

Giovanni Occhipinti,[1,2] Philippe Lognonné,[1] E. Alam Kherani,[1] and Hélène Hébert[3]

Received 11 May 2006; revised 11 July 2006; accepted 31 July 2006; published 21 October 2006.

[1] The Sumatra, December 26th, 2004, tsunami produced internal gravity waves in the neutral atmosphere and large disturbances in the overlying ionospheric plasma. To corroborate the tsunamigenic hypothesis of these perturbations, we reproduce, with a 3D numerical modeling of the ocean-atmosphere-ionosphere coupling, the tsunami signature in the Total Electron Content (TEC) data measured by the Jason-1 and Topex/Poseidon satellite altimeters. The agreement between the observed and synthetic TEC shows that ionospheric remote sensing can provide new tools for offshore tsunami detection and monitoring. **Citation:** Occhipinti, G., P. Lognonné, E. A. Kherani, and H. Hébert (2006), Three-dimensional waveform modeling of ionospheric signature induced by the 2004 Sumatra tsunami, *Geophys. Res. Lett.*, *33*, L20104, doi:10.1029/2006GL026865.

1. Introduction

[2] Several theoretical studies in the 70s, including Hines's pioneering works on internal gravity waves (IGWs), suggested that atmospheric IGWs are generated by a tsunami and may well produce identifiable ionospheric signatures in the plasma [*Hines*, 1972; *Peltier and Hines*, 1976]. Ionospheric radio sounding or imaging might therefore be another possible technique for tsunami observations. In essence, electromagnetic waves interact with electrons present in the plasma, and their propagation is affected by anomalies induced by tsunami-coupled IGWs in the Earth's ionosphere. The first tsunami-related ionospheric observation followed the tsunamigenic Mw = 8.2 quake in Peru (June 23th, 2001) [*Artru et al.*, 2005a]. Ionospheric traveling waves, identified *via* total electron content (TEC), were observed by the GPS dense Japanese network (GEONET) and presented an azimuth and arrival time coherent with the tsunami's propagation. A period between 22 and 33 min, coherent with the tsunami, was identified in the observed TEC signals but no forward modeling has been done to discriminate between traveling ionospheric disturbances (TIDs) [*Aframovich et al.*, 2003; *Balthazor and Moffet*, 1997] and tsunami generated IGWs. The Sumatra, Mw = 9.3, tsunami of December 26th, 2004 [*Lay et al.*, 2005] (0:58:50 UT, 3.3N, 95.8E) was about one order of magnitude larger. In addition to seismic waves detected by global seismic networks [*Park et al.*, 2005], infrasound and gravity waves [*Le Pichon et al.*, 2005], magnetic [*Iyemori et al.*, 2005] and ionospheric anomalies have been reported [*Liu et al.*, 2006a, 2006b; *Lognonné et al.*, 2006; *Artru et al.*, 2005b; *DasGupta et al.*, 2006]. In the north of Sumatra, the latter have been associated with Rayleigh waves and atmospheric gravity waves [*Liu et al.*, 2006a]. In the south, TEC perturbations has been observed by GPS [*Liu et al.*, 2006b; *Lognonné et al.*, 2006] with arrival times coherent with the tsunami's propagation [*Liu et al.*, 2006b]. Key observations of the Sumatra tsunami were performed by the Topex/Poseidon and Jason-1 sea altimetry satellites. The measured sea level displacements is well explain by tsunami propagation models with realistic bathymetry, and provided useful constraints in the source mechanism inversion [e.g., *Song et al.*, 2005]. In addition, the inferred TEC data, required to remove the ionospheric effects from the altimetric measurements [*Bilitza et al.*, 1996], show strong anomalies in the integrated electron density [*Artru et al.*, 2005b]. These anomalies reach about 3–5 *TECU* [$1 TECU = 10^{16} e^{-}/m^{2}$]. GPS anomalies shown by *DasGupta et al.* [2006] are comparable and those detected by *Liu et al.* [2006b] lead to peak-to-peak differential slant TEC values of about 0.4 *TECU*/30*sec*.

[3] All these observations have clearly confirmed that the tsunami generates large ionospheric perturbations. We perform here a complete modeling of tsunami propagation from the source to the top of ionosphere. We focused on the TEC perturbations detected by Jason-1 and Topex/Poseidon, leaving those detected by GPS for a future paper. The synthetic TEC is reproduced *via* a 3D numerical computation based on the primary coupling mechanisms between the ocean displacement, neutral atmosphere and plasma. To our knowledge, this is the first time that tsunami TEC signature is reproduced with a good agreement with data. We then discuss how a high resolution ionospheric monitoring may complete future tsunami warning systems based on the seismic alert and other more classical and proven in-situ techniques (e.g. buoys, ocean bottom pressure gauges, tide gauges).

2. Modeling

[4] The modeling of synthetic TEC data is divided into three steps (Figure S1[1]). First, we compute the tsunami propagation using a realistic bathymetry of the Indian ocean. Second, the computed tsunami oceanic displacement is used as the excitation source of IGWs in the neutral atmosphere (Figure 1a and Animation S1). Finally, we compute the response of the ionosphere induced by the neutral atmospheric motion (Figure 1b and Animation S2

[1]Institut de Physique du Globe de Paris (UMR-7154), Paris, France.
[2]Also at ONERA, DEMR/RBF, Palaiseau, France.
[3]CEA/DASE, Bruyères-le-Chatel, France.

0094-8276/06/2006GL026865

[1]Auxiliary materials are available in the HTML. doi:10.1029/2006gl026865.

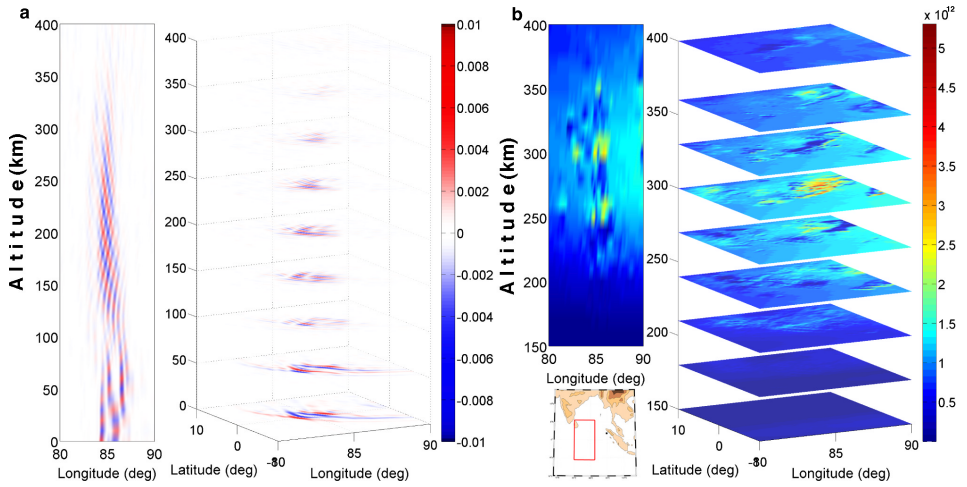

Figure 1. Tsunami-generated IGWs and the response of the ionosphere to neutral motion at 2:40 UT. (a) The normalized vertical velocity $V_z\sqrt{\rho_0}$ ($\sqrt{\frac{kg}{m}}s^{-1}$) induced by tsunami-generated IGWs in the neutral atmosphere is shown. The normalisation $\sqrt{\rho_0}$ (where ρ_0 is the neutral atmosphere background density [*Picone et al.*, 2002]) is used here in order to show the perturbation at all altitudes. Between 250 and 350 km of altitude, the effect of neutral-plasma coupling is maximum, and typical perturbations induced by the Sumatra tsunami are of the order of 500–600 m/s for vertical and horizontal components of IGWs. (b) We show the perturbation induced by IGWs in the ionospheric plasma (e/m^3), the transient wake is clearly distinguished from the ionospheric background and has a maximum located around 300 km of altitude. The vertical cut in Figures 1a and 1b is at $-1°$ of latitude.

and, by vertical integration, the synthetic TEC (Figure 2 and Animation S3).

2.1. Tsunami Propagation

[5] The modelling of ocean see surface displacement is carried out using a finite difference scheme that resolves the hydrodynamical equations on a 2' bathymetric grid. The input earthquake source consists of 3 subfaults describing the whole 2004 rupture with fault slip ranging from 4 to 20 m in the southern extremity. Similar sources were successfully used to model the impact of the tsunami in La Réunion [*Hébert et al.*, 2006].

2.2. Tsunami-Neutral Atmosphere Coupling

[6] The theoretical coupling between tsunami and internal gravity waves uses the ocean displacement to excite atmospheric IGWs. The linearised momentum and continuity equations, for irrotational, inviscid and incompressible flow [*Nappo*, 2002], are used here to describe the gravity wave propagation by the way of a vertical propagator $\frac{dV}{dz} = AV$ with:

$$V = \begin{pmatrix} \sqrt{\rho_0}\tilde{u}_{z(k_x,k_y,\omega)} \\ \frac{1}{\sqrt{\rho_0}}\tilde{P}_{(k_x,k_y,\omega)} \end{pmatrix}$$

$$A = \begin{pmatrix} 0 & \frac{1}{2}\frac{d\ln\rho_0}{dz} - \frac{i\left(k_x^2+k_y^2\right)}{\omega} \\ i\left(\omega + \frac{g}{\omega}\frac{d\ln\rho_0}{dz}\right) & -\frac{1}{2}\frac{d\ln\rho_0}{dz} \end{pmatrix}$$

In essence, the ocean surface displacement in the spectral domain (couched here by vertical velocity $\tilde{u}_z(k_x, k_y, \omega)$ and

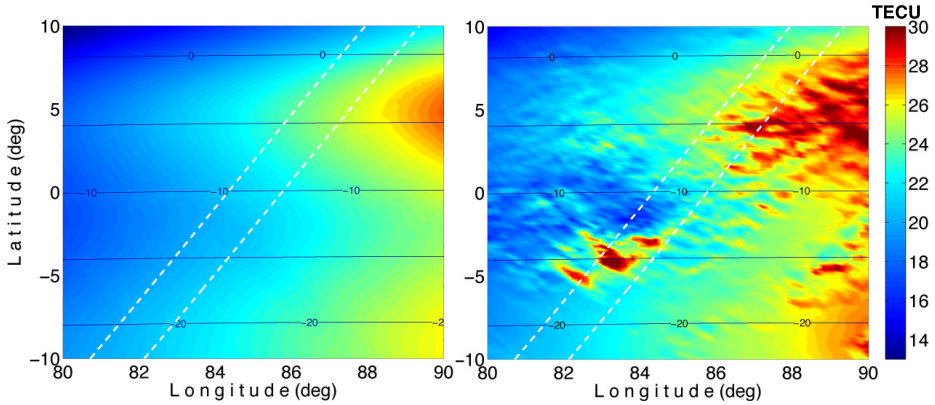

Figure 2. Tsunami signature (right) in the TEC at 3:18 UT and (left) the unperturbed TEC. The TEC images have been computed by vertical integration of the perturbed and unperturbed electron density fields (e.g., Figure 1b). The TEC perturbation induced by tsunami-coupled IGW is superimposed on a broad local-time (sunrise) TEC structure. The broken lines represent the Topex/Poseidon (left) and Jason-1 (right) trajectories. The blue contours represent the magnetic field inclination.

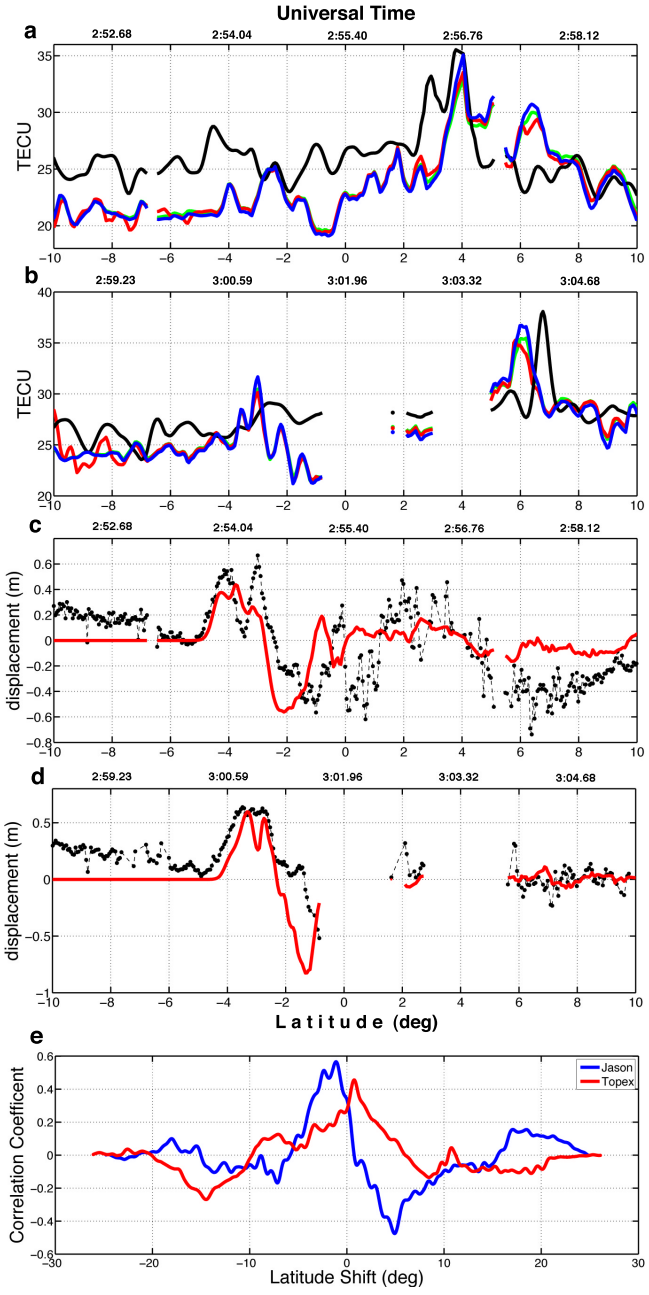

Figure 3. Altimetric and TEC signatures of the Sumatra tsunami. The modelled and observed TEC are shown for (a) Jason-1 and (b) Topex/Poseidon: data (black), synthetic TEC without production-recombination-diffusion effects (blue), with production-recombination (red), and production-recombination-diffusion (green). The Topex/Poseidon synthetic TEC has been shifted up by 2 TEC units. (c and d) The altimetric measurements of the ocean surface (black) are plotted for the Jason-1 and Topex/Poseidon satellites, respectively. The synthetic ocean displacements, used as the source of IGWs in the neutral atmosphere, are shown in red. For each plot from Figures 3a to 3d, the latitude and corresponding Universal Time are shown. (e) Cross correlation between TEC synthetics and data are shown for Jason (blue) and Topex/Poseidon (red).

pressure $\tilde{P}(k_x, k_y, \omega)$ fields) is injected as a forcing term in the unperturbed neutral atmosphere. The perturbation is, therefore, propagating upward for triplets (k_x, k_y, ω) inducing a positive k_z. In other words the effect of IGWs on the tsunami itself and all evanescent waves are neglected. A 1D non-isothermal atmosphere with horizontal stratification consistent with an *a priori* density profile ρ_0 depending on geographical position (0^o North, 85^o East) and local time (3:00 UT) is used [*Picone et al.*, 2002].

2.3. Neutral-Plasma Coupling

[7] IGWs are known to produce irregularities in the ionospheric plasma (e.g. TIDs) and some studies of the nature of neutral-plasma coupling have been made in the past utilizing different assumptions [*Hooke*, 1968; *Davis*, 1973]. We use here a non-linear 3D ionospheric simulation model based on the space-time finite-differences [*Kherani et al.*, 2004, 2006] and solving the hydro-magnetic equations [*Kelley*, 1989] (equations (1) and (2)) for three ions-*i* (O_2^+, NO^+ and O^+) under the effect of IGWs (Figure 1b). The large periods of IGWs allows to neglected the acceleration term (left side of equation (2)).

$$\frac{\partial n_i}{\partial t} + \nabla \cdot (n_i \vec{v}_i) = \pm \beta n_i - \alpha n_i^2 \tag{1}$$

$$\rho_i \frac{d\vec{v}_i}{dt} = 0 = -\nabla p_i + \rho_i \vec{g} + n_i q_i \left(\vec{E} + \vec{v}_i \times \vec{B}\right) - \rho_i \mu_{in} (\vec{v}_i - \vec{v}_n) \tag{2}$$

Physically, the neutral atmospheric motion v_n induces fluctuations in the plasma velocity v_i by wind share mechanism [*Schunk and Nagy*, 2000]. The momentum transfer is primarily dominated by the frictional term driven by collision frequency μ_{in} and by the Lorentz term associated with the Earth magnetic and electric field ($\vec{B}$ and $\vec{E}$). Ion loss α (= 0 for O^+), recombination β (with negative sign for $O+$ and positive sign for O_2^+ and NO^+) and diffusion (implicit in p_i) are also taken into account in the ionic continuity equation (1), but their role is negligible. Finally, the perturbed electron density n_e is extrapolated from ion densities n_i using the hypothesis of charge neutrality $n_e = \Sigma n_i$. The 3D ionosphere is based on the IRI model [*Bilitza*, 2001] at 3:00 UT for electron density, the SAMI model [*Huba et al.*, 2000] for collision, production and loss ion parameters and the IGRF model (F. J. Lowes, The International Geomagnetic Reference Field: A health warning, http://www.ngdc.noaa.gov/IAGA/vmod/igrfhw.html) for the geo-magnetic field.

3. Result

[8] Our simulation shows that about one hour after the tsunami generation, most of the energy in the tsunami-generated IGW reaches the altitude of 300 km, where the value of the electron density becomes significant (Figure 1a and Animation S1). The IGW's upward propagation time depends on the tsunami period, T, and wavelength, λ; the latter being related to the depth of the ocean [*Satake*, 2002]. This dispersive effect in the upward velocity modifies the tsunami waveform during its propagation from the ocean

surface to high altitudes. The ionospheric response to the IGW forcing is instantaneous, and produces an transient wake (Figure 1b) that disappears with the diffusion and chemical loss time scale (few hours). In contrast to diffusion, ion-production and loss effects, the magnetic latitude plays a crucial role: the signature of IGWs in the plasma is maximized in the direction of magnetic field. As the horizontal components of tsunami generated IGWs are generally larger than vertical ones, the large TEC anomaly detected by Topex/Poseidon and Jason-1 near the magnetic equator (8°North) is probably generated by the synergy of the horizontal magnetic field and the equatorial ionisation anomaly (EIA). This first perturbation appears one hour after the fault breaking (Figure 2 and Animation S3) and is observed on the data. A second perturbation, located near 5° South, is induced by fully developed IGWs in the ionosphere and appears only after the transit of both satellites (Animation S3). Moreover, Figure 2 resumes the geometrical structure of TEC tsunami signature: in the regions ran over by IGWs, the relative amplitude of perturbations reaches 10% of local unperturbed TEC. The equivalent differential TEC is in order of 0.2–0.6 *TECU*/30*sec*, coherent with [*Liu et al.*, 2006b].

[9] In Figures 3a and 3b the simulated TEC along the Topex/Poseidon and Jason-1 trajectories are compared with data. For complicity, synthetic displacements at the ocean surface and altimetric data are shown for both satellites (Figures 3c and 3d). The observed and simulated TEC is fairly good in agreement: the position of the principal peaks (around 4°N for Jason-1 and 7°N for Topex/Poseidon), the agreement in the complete waveform (in particular for Jason-1), as well as the perturbation's amplitudes are the most important validations of our modeling. A more quantitative analysis by cross-correlation shows that the synthetics and data are in agreement with a shift of −1.1° and 0.75° for Jason-1 and Topex/Poseidon respectively (Figure 3e). The observed shifts confirm the presence of zonal and meridional wind neglected in our modeling. Other disagreements between synthetics and data are related, in our opinion, to the chosen seismic source and principally to differences between the *a priori* and real electron density background above all in the EIA [*Bilitza et al.*, 1996].

4. Conclusion

[10] Notwithstanding the differences between synthetics and data, the tsunami signature in the TEC observed by Topex/Poseidon and Jason-1 is clearly identified, not only for arrival times and positions, but also for waveforms and amplitudes. This shows that the process transferring the tsunami energy into the ionosphere can be modeled and, in this way, very exciting perspectives are opened in offshore tsunami detection. The ionospheric monitoring by ground/space techniques (Doppler sounding, over the horizon radars, GPS networks, airglow satellites observations, etc.) combined with seismic networks and tide gauges can open new insights into the development of efficient tsunami monitoring and warning systems. Moreover, the Topex/Poseidon and Jason-1 data represent only one snapshot of the ionospheric perturbation. Therefore, we can expect that continuous monitoring will be able to image tsunami-generated ionospheric anomalies in space and time.

[11] **Acknowledgments.** This project is supported by the French ANR under contract CATELL-IONONAMI, by CNES and by the French Ministry of Research. We thank J.B. Minster and an anonymous reviewer for their constructive remarks and the allowed slight pinch of liberty. We thank NRL for development of SAMI2 software. This is IPGP contribution 2154.

References

Aframovich, E. L., N. P. Perevalova, and S. V. Voyeikov (2003), Traveling wave packets of total elctron content disturbances as deduced from GPS network data, *J. Atmos. Sol. Terr. Phys.*, *65*, 1245–1262.

Artru, J., V. Ducic, H. Kanamori, P. Lognonné, and M. Murakami (2005a), Ionospheric detection of gravity waves induced by tsunamis, *Geophys. J. Int.*, *160*, 840–848.

Artru, J., P. Lognonné, G. Occhipinti, F. Crespon, R. Garcia, E. Jeansou, and M. Murakami (2005b), Tsunamis detection in the ionosphere, *Space Res. Today*, *163*, 23–27.

Balthazor, R. L., and R. J. Moffet (1997), A study of atmospheric gravity waves and travelling ionospheric disturbances at equatorial latitude, *Ann. Geophys.*, *15*, 1048–1056.

Bilitza, D. (2001), International Reference Ionosphere 2000, *Radio Sci.*, *36*(2), 261–275.

Bilitza, D., C. Koblinsky, S. Zia, R. Williamson, and B. Beckley (1996), The equator anomaly region as seen by the TOPEX/Poseidon satellite, *Adv. Space Res.*, *18*(6), 23–32.

DasGupta, A., A. Das, D. Hui, K. K. Bandyopadhyay, and M. R. Sivaraman (2006), Ionospheric perturbation observed by the GPS following the December 26th, 2004 Sumatra-Andaman earthquake, *Earth Planets Space*, *35*, 929–959.

Davis, M. J. (1973), The integrated ionospheric response to internal atmospheric gravity waves, *J. Atmos. Terr. Phys.*, *35*, 929–959.

Hébert, H., A. Sladen, and F. Schindelé (2006), Numerical modeling of the great 2004 Indian Ocean tsunami: Focus on the Mascarene Islands, *Bull. Seismol. Soc. Am.*, in press.

Hines, C. O. (1972), Gravity waves in the atmosphere, *Nature*, *239*, 73–78.

Hooke, W. H. (1968), Ionospheric irregularities produced by internal gravity waves, *J. Atmos. Terr. Phys.*, *30*, 795–823.

Huba, J. D., G. Joyce, and J. A. Fedder (2000), Sami2 is Another Model of the Ionosphere (SAMI2): A new low-latitude ionosphere model, *J. Geophys. Res.*, *105*(A10), 23,035–23,054.

Iyemori, T., et al. (2005), Geomagnetic pulsations caused by the Sumatra earthquake on December 26, 2004, *Geophys. Res. Lett.*, *32*, L20807, doi:10.1029/2005GL024083.

Kelley, M. C. (1989), *The Earth's Ionosphere, Plasma Physics and Electrodynamics*, *Int. Geophys. Ser.*, vol. 43, Elsevier, New York.

Kherani, E. A., E. R. de Paula, and F. C. P. Bertoni (2004), Effects of the fringe field of Rayleigh-Taylor instability in the equatorial E and valley regions, *J. Geophys. Res.*, *109*, A12310, doi:10.1029/2003JA010364.

Kherani, E. A., M. Mascarenhas, J. H. A. Sobral, Eurico R. de Paula, and F. C. Bertoni (2006), A three dimension simulation of collisional-interchange-instability in the equatorial-low-latitude ionosphere, *Space Sci. Rev.*, in press.

Lay, T., et al. (2005), The great Sumatra-Andaman earthquake of 26 December 2004, *Science*, *308*, 1127–1133.

Le Pichon, A., P. Herry, P. Mialle, J. Vergoz, N. Brachet, M. Garcs, D. Drob, and L. Ceranna (2005), Infrasound associated with 2004–2005 large Sumatra earthquakes and tsunami, *Geophys. Res. Lett.*, *32*, L19802, doi:10.1029/2005GL023893.

Liu, J. Y., Y. B. Tsai, S. W. Chen, C. P. Lee, Y. C. Chen, H. Y. Yen, W. Y. Chang, and C. Liu (2006a), Giant ionospheric distrubances excited by the M9.3 Sumatra earthquake of 26 December 2004, *Geophys. Res. Lett.*, *33*, L02103, doi:10.1029/2005GL023963.

Liu, J., Y. Tsai, K. Ma, Y. Chen, H. Tsai, C. Lin, M. Kamogawa, and C. Lee (2006b), Ionospheric GPS total electron content (TEC) disturbances triggered by the 26 December 2004 Indian Ocean tsunami, *J. Geophys. Res.*, *111*, A05303, doi:10.1029/2005JA011200.

Lognonné, P., J. Artru, R. Garcia, F. Crespon, V. Ducic, E. Jeansou, G. Occhipinti, J. Helbert, G. Moreaux, and P. E. Godet (2006), Ground based GPS imaging of ionospheric post-seismic signal, *Planet. Space Sci.*, *54*, 528–540.

Nappo, C. J. (2002), *An Introduction to Atmospheric Gravity Waves*, *Int. Geophys. Ser.*, vol. 85, 26 pp., Elsevier, New York.

Park, J., K. Anderson, R. Aster, R. Butler, T. Lay, and D. Simpson (2005), Global Seismographic Network records the Great Sumatra-Andaman earthquake, *Eos Trans. AGU*, *86*(6), 60.

Peltier, W. R., and C. O. Hines (1976), On the possible detection of tsunamis by a monitoring of the ionosphere, *J. Geophys. Res.*, *81*(12), 1995–2000.

Picone, J. M., A. E. Hedin, D. P. Drob, and A. C. Aikin (2002), NRLMSISE-00 empirical model of the atmosphere: Statistical compari-

sons and scientific issues, *J. Geophys. Res.*, *107*(A12), 1468, doi:10.1029/2002JA009430.

Satake, K. (2002), Tsunamis, in *International Handbook of Earthquake and Engineering Seismology, Part A*, *Int. Geophys. Ser.*, vol. 81A, edited by W. H. K. Lee et al., pp. 437–451, Elsevier, New York.

Schunk, R. W., and A. F. Nagy (2000), *Ionospheres*, Cambridge Univ. Press, New York.

Song, Y. T., C. Ji, L.-L. Fu, V. Zlotnicki, C. K. Shum, Y. Yi, and V. Hjorleifsdottir (2005), The 26 December 2004 tsunami source estimated from satellite radar altimetry and seismic waves, *Geophys. Res. Lett.*, *32*, L20601, doi:10.1029/2005GL023683.

H. Hébert, CEA, DASE/LDG, BP 12, F-91680 Bruyères-le-Chatel, France.

E. A. Kherani, P. Lognonné, and G. Occhipinti, Institut de Physique du Globe de Paris, 4, av. de Neptune, F-94107 Saint Maur Cedex, France. (occhip@ipgp.jussieu.fr)